Spiro-graphene: a two-dimensional metallic carbon allotrope of fused pentagons

Susumu Okada[a,*], Nguyen Thanh Cuong[a], Yanlin Gao[a], Mina Maruyama[a]

[a]*Department of Physics, Graduate School of Pure and Applied Sciences, University of Tsukuba, 1-1-1 Tennodai, Tsukuba, Ibaraki 305-8571, Japan*

Abstract

Using density functional theory with the generalized gradient approximation, we explored the geometric and electronic structure of polymerized spiro[4,4]nonatetraene (spiro-graphene) as a possible two-dimensional carbon allotrope comprising sp^2 and sp^3 C atoms. By reflecting a shape of the hydrocarbon molecule, this two-dimensional allotrope has a covalent network of fused pentagons with nanometer-scale structural rippling. The covalent network is thermally and dynamically stable with a relatively high total energy, higher than graphene by 0.6 eV/atom. The spiro-graphene is a metal where two linear dispersion bands cross each other at the Fermi level. In addition to these linear dispersion bands, the covalent network possesses the Dirac nodal line just above the Fermi level and along the Brillouin zone boundary. Accordingly, the ribbons with zigzag edges derived from spiro-graphene possess edge states like those of graphene nanoribbons with zigzag edges.

Keywords: 2D C allotrope, Spiro-carbon, Dirac nodal line, Edge state

*Corresponding author
Email address: sokada@comas-tsukuba.jp (Susumu Okada)

1. Introduction

Electrons distributed on a honeycomb network of sp^2 C atoms cause conical dispersion bands at the six corners of the hexagonal Brillouin zone and around the Fermi level[1, 2, 3]. This peculiar electronic band structure makes graphene a unique material, exhibiting an unusual quantum Hall effect and possessing remarkable carrier mobility [4, 5, 6, 7]. The honeycomb network of π electrons also causes peculiar electronic structures by introducing imperfections, such as defects and edges, owing to the broken symmetry of the bipartite network. Graphene with atomic defects possess versatile electronic structures, ranging from metallic to semiconducting, depending on their shape and arrangement [8, 9, 10, 11, 12, 13]. Edges with zigzag shape caused peculiar edge localized states at those atomic sites and at the Fermi level owing to the delicate balance of the π electron transfer through the networks [14, 15, 16, 17]. In addition, topological defects, e.g., pentagons and heptagons, highly modulate the characteristic electronic structure of graphene [18, 19, 20, 21, 22]. Indeed, a two-dimensional sp^2 network of fused pentagons possessed a flat dispersion band in a part of the hexagonal Brillouin zone with nonbonding nature that caused spin polarization throughout the networks, even though all C atoms were electronically saturated [22]. Furthermore, tubular boundary conditions imposed on the graphene strips produce carbon nanotubes, whose electronic structures are determined by the atomic arrangements along their circumferences [23, 24, 25].

Topological design of sp^2 C atoms provided an additional degree of freedom to tune the electronic structure of carbon-based nanoscale materials because the covalent network topologies of sp^2 C atoms tightly correlated with their electronic structure. Polymerization of small hydrocarbon molecules is one of plausible pro-

cedure for synthesizing covalent networks of C atoms whose structures are precisely controlled. Indeed, size- and shape-controlled graphene nanoribbons and nanoplates have been synthesized from hydrocarbon molecules on metal surfaces by polymerization at elevated temperature [26, 27, 28]. Polymerization of hydrocarbon molecules in appropriate solutions leads to two- and three-dimensional covalent networks in which the constituent molecules are basically connected via single bonds [29, 30, 31, 32]. These procedures benefit from the ability to design the electronic structures of resultant covalent networks by assembling and polymerizing appropriate molecules. A copolymer of phenalenyl and phenyl, which are alternately arranged in a hexagonal manner, has an interesting electronic structure near the Fermi level, with a narrow Dirac cone at the Fermi level and kagome bands above and below the Fermi level, resulting from the molecular orbitals of the constituent units [13].

In this work, we aim to investigate the geometric and electronic structure of a two-dimensional covalent network of fused pentagons with structural rippling using density functional theory (DFT) with generalized gradient approximation (GGA) because the pentagonal rings and polymeric structure of hydrocarbon molecules lead to a peculiar electronic structure. We focus on a fenestratetraene framework (four pentagons sharing their edges and one vertex) as a constituent unit of the network [33, 34, 35]. Indeed, a saddle-shaped polycyclic aromatic compound has been synthesized containing this framework [36, 37, 38]. By extending the network using this framework, we can straightforwardly obtain the two-dimensional covalent network of fused pentagons of sp^2 and sp^3 C atoms. Our DFT calculations revealed that the network is a metastable phase of a metallic carbon allotrope with relatively high total energy and remarkable thermal

stability. Furthermore, because of the bipartite network of fused pentagons, the pentagonal network has a Dirac nodal line just above the Fermi level and along the two-dimensional Brillouin zone boundary. Accordingly, a nanoribbon with zigzag edges derived from this network has edge localized states whose wave function distribution shows similar characteristics to those of graphene nanoribbons with zigzag edges.

2. Calculation methods

Geometric and electronic structures of a fused pentagonal network of sp^2 and sp^3 C atoms were investigated using DFT [39, 40] implemented in the program package STATE [41, 42] and Quantum Espresso [43]. The exchange-correlation potential energy among interacting electrons is treated by the generalized gradient approximation with the Perdew–Burke–Ernzerhof functional [44]. An ultrasoft pseudopotential is adopted to describe the interactions between electrons and nuclei [45]. The valence wave function and deficit charge density in the core region are expanded in terms of the plane wave basis sets with cutoff energies of 25 Ry and 225 Ry, respectively. Integration over the two-dimensional Brillouin zone was carried out using equidistant 8×8 $\boldsymbol{k}$-meshes, which were used for the self-consistent electronic structure calculations. Lattice parameters and internal atomic coordinates were optimized until the force acting on each atom became less than 5 mRy/Å.

3. Results and Discussion

Figure 1(a) shows an optimized structure of a two-dimensional covalent network of fused pentagons of sp^2 and sp^3 C atoms derived from the polymerization

of spiro[4,4]nonatetraene [46, 47, 48]. In this two-dimensional covalent network, spiro[4,4]nonatetraene are alternately arranged with two different molecular orientations, resulting in the orthorhombic lattice with the periodic concave–convex structure of sp^2 C rings. Accordingly, for a network topology of sp^2 C atoms, the covalent network is regarded as a face-centered square lattice of C_8 rings that are connected to their four adjacent C_8 rings. Therefore, the topological network of sp^2 C atoms form a bipartite lattice with internal degrees of freedom, which may exhibit unusual physical properties.

Table 1: Optimized atomic coordinates, lattice constants, and space group symmetry of polymerized spiro[4,4]nonatetraene. Atom indexes are defined in Fig. 1.

Pmmn	$a = b$ =6.615 Å	c =10.000 Å	
C1	0.0000	0.0000	0.0000
C2	0.0000	–0.21549	0.06328
C3	–0.18850	–0.31160	0.04317
C4	–0.21549	0.00000	–0.06328

Optimized atomic coordinates of the polymerized spiro[4,4]nonatetraene are listed in Table I. The optimized lattice parameters of a and b are 6.615 Å, which are equal because of the alternating arrangement of spiro[4,4]nonatetraene. The atomic density of this covalent network under the optimized lattice parameters is 0.411 atom/Å^2, which is lower than that of graphene (0.661 atom/Å^2). This low density is attributed to the large pore of the C_8 rings of sp^2 C atoms, even though the network consisted of fused pentagons containing sp^3 C atoms and contained structural rippling. The optimized bond lengths of the fused pentagonal covalent network are 1.560 Å, 1.414 Å, and 1.439 Å for C1-C2/C1-C4, C2-C3/C3-C4, and

C3-C3, respectively. The results indicated that bonds associated with C1 are close to those of the sp^3 C atom in diamond and that the bonds associated with the three-fold coordinations (C2, C4, and C3) are close to those of graphene. In contrast, the fused pentagonal network led to substantial distortion in bond angles from those of ideal sp^2 and sp^3: Bond angles of θ_{C1C2C3}, θ_{C2C1C4}, θ_{C2C1C2}, θ_{C2C3C3}, θ_{C2C3C4}, and θ_{C3C2C3} are 110.6°, 99.4°, 132.1°, 109.2°, 140.5°, and 123.7°, respectively.

Figure 2 shows the relative total energy per atom of polymerized spiro[4,4]nonatetraene as a function of the atomic area with respect to that of graphene. This network has an energy minimum at the lattice constant $a = b$ =6.615 Å with the relative energy of 619 meV/atom, which is higher than that of C_{60} by approximately 200 meV, but still lower than that of the fused acepentalene sheet by approximately 100 meV. Thus, this result confirms that the polymerized spiro[4,4]nonatetraene is a potential metastable phase of two-dimensional carbon allotropes comprising three- and four-fold coordinated C atoms. The relatively higher total energy is attributed to the highly distorted bond angles of the three- and four-fold coordinated C atoms. The distorted bond angles also make the polymerized spiro[4,4]nonatetraene a softer material than graphene.

In addition to energetic stability, we investigated the thermal or dynamical stability. We first investigated the phonon dispersion relation of the polymerized spiro[4,4]nonatetraene using the density functional perturbation theory method [49] implemented in the Quantum Espresso code [Fig. 3(a)]. The calculated phonon dispersion does not have any soft vibrational mode, confirming its dynamical stability. The dynamical/thermal stability is also investigated by carrying out ab initio molecular dynamics (MD) simulations on the polymerized spiro[4,4]nonatetraene under the $\sqrt{2} \times \sqrt{2}$ cell with the velocity scaling method

to maintain the temperature at 2000 K and 4000 K during the simulations. The polymer retained the initial covalent network topology for 10 ps at T = 2000 K [Fig. 3(b)]. In comparison, the polymerized spiro[4,4]nonatetraene hardly retains its initial covalent network for 10 ps at T = 4000 K [Fig. 3(c)]. Therefore, the phonon dispersion and MD simulations confirmed that the polymerized spiro[4,4]nonatetraene is thermally and energetically stable once synthesized using appropriate experimental procedures. It is worth to discuss the possibility of structural transition from spiro-graphene to other related structures which possess the same core sp^3 C structure [50, 51]. The structural transition to tetrahexcarbon or C_{568} structures is hardly to occur owing to the density difference of sp^3 C atoms between spiro-graphene and these structures, because the migration of sp^3 C atoms on the sheets required much energy cost associated with the bond dissociation and formation. Therefore, in this view, the spiro-graphene is stable carbon allotrope, although it has the similar total energy to that of the tetrahexcarbon and C_{568}.

We investigated the formation energy ΔE of polymerized spiro[4,4]nonatetraene from a simplified polymerization reaction because the polymeric form has thermal and energetic stability.

$$2 \times \text{spiro}[4,4]\text{nonatetraene} = \text{polymer} + 8 \times H_2 + \Delta E$$

The calculated formation energy was 7.16 eV, which corresponds to the energy cost to extend a covalent network of sp^2 with distorted bond angles. This large amount of energy implies that the direct polymerization of spiro[4,4]nonatetraene rarely occurs. Thus, appropriate intermediates, such as Br substituted derivatives, are required to achieve the polymerized structure with the aid of cross-coupling procedures.

Figure 4 shows the electronic energy band of polymerized spiro[4,4]nonatetraene. The polymer is a metal where the dispersive band and moderate dispersive band cross each other at the Fermi level and the middle of orthorhombic Brillouin zone. Accordingly, the polymer has an approximately circular Fermi circle. The two bands crossing each other have a linear dispersion relation at the Fermi level because the Fermi level is located in the middle of the Brillouin zone. Note that these Dirac electrons at the Fermi level are attributed to accidental conditions, and are not symmetrical conditions. Wave functions of the states crossing the Fermi level possess π nature, so this metallic C sheet is a possible candidate of a π electron system with structural rippling [Fig. 5(a)]. Linear dispersion bands at the Fermi level and the Fermi circle may have caused the remarkable carrier mobility in this covalent network of sp^2 and sp^3 C atoms.

One of two linear dispersion bands at the Fermi level retains its linearity through the X point, producing the other Dirac bands along the Brillouin zone boundary (Fig. 4). Wave functions of these states at the X point are alternately distributed on atoms with three-fold coordination, exhibiting similar characteristics to the wave function distribution of graphene at the Dirac point [Fig. 5(b)]. Thus, these Dirac states are topologically induced by the atomic arrangement of three-fold coordinated C atoms in the sheet. Furthermore, the two states are degenerate along the zone boundary from the X to M. The Dirac states and doubly degenerate flat bands at the zone boundary are attributed to the band folding of the two-dimensional cosine band of $1/\sqrt{2}\times 1/\sqrt{2}$ face-centered square lattice into the present 1×1 lattice because the π electron network is approximately regarded as a flat topological network[Fig. 4(b)]. Therefore, the sp^3 atoms in the polymerized network make the π network a bipartite system. Accordingly, the linear dispersion

relation at the zone boundary is retained except at the M point which corresponds with the saddle point of the two-dimensional cosine band.

Topologically induced Dirac states occasionally caused edge localized modes like the edge states in graphene nanoribbons with zigzag edges. We considered the nanoribbons of polymerized spiro[4,4]nonatetraene with zigzag and armchair edges to explore the possibility of edge localized mode (Fig. 6). As mentioned above, the polymerized spiro[4,4]nonatetraene is a bipartite network of spiro[4,4]nonatetraene, which is alternately arranged in orthorhombic symmetry with interunit sp^2 covalent bonds; simultaneously, the three-fold coordinated C atoms also form a bipartite network. Thus, the edges of the zigzag ribbon contain only one of two atomic sublattices or spiro[4,4]nonatetraene units, like zigzag graphene nanoribbons. In contrast, the armchair edges contain both atomic sublattices or spiro[4,4]nonatetraene units.

Figure 7 shows the electronic energy band of the nanoribbons. The ribbon with zigzag edges is a metal whose band structure is mostly interpreted by projecting the band structure of the two-dimensional sheet on the ribbon direction, with appropriate discretization of the wave number normal to the ribbon direction. Owing to the band projection, four bands associated with the Dirac state emerge just above the Fermi level. Two of four bands have substantial dispersion and correspond with the Dirac bands along the Γ-X line of the two-dimensional sheet. However, the states corresponding to the doubly degenerate states of the two-dimensional sheet split into upper and lower branches: one retains its flat band nature along the ribbon with a width of 0.1 eV while the other has substantial dispersion. Wave functions of these states exhibit characteristic features of the edge state. These states are extended across the ribbons at the Γ point, while

approximately localized at the edge atomic site at the X point. Thus, the symmetry breaking at the zigzag edges causes the edge localized states, as is occurs with graphene. In contrast to the ribbon with zigzag edges, the ribbon with armchair edges does not have a such peculiar edge mode. The energy bands could be interpreted as simple band projection, and their wave function does not show the edge localized nature at the Γ and X points.

4. Conclusion

Using the DFT with GGA, we predicted the possible two-dimensional covalent network of fused pentagonal rings consisting of sp^2 and sp^3 C atoms produced by polymerizing spiro[4,4]nonatetraene. The two-dimensional covalent network is a plausible metastable carbon allotrope whose total energy is higher by 0.61 eV/atom than that of graphene owing to the substantial distortion of bond angles from those of ideal sp^2 and sp^3 C atoms. The polymer is dynamically and thermally stable, as confirmed by phonon calculations and first principle MD simulations, although the polymer does have relatively high total energy. The polymer is a metal with liner dispersion bands at the Fermi level. In addition, because of the bipartite network of fused pentagons, the fused pentagonal network has a Dirac nodal line just above the Fermi level and along the two-dimensional Brillouin zone boundary. Therefore, the two-dimensional network may exhibit unusual electronic properties by injecting electrons up to the Dirac nodal line. In particular, the remarkable carrier mobility is expected owing to the finite density of states at the Dirac nodal line under the electron doping. The nanoribbons derived from the polymerized spiro[4,4]nonatetraene are also studied in terms of their edge structures. Owing to the Dirac nodal line along the Brillouin zone

boundary, the nanoribbon with zigzag edges has edge localized states with a flat dispersion band whose wave function distribution is perfectly localized at the edge atomic site at the Brillouin zone boundary and is extended throughout the ribbons for the rest of the wave numbers. In contrast, the electronic energy band of the ribbon with armchair edges is obtained by band folding on the energy band of the two-dimensional sheet. These results imply that the nanoribbon with zigzag edges exhibits unusual physical phenomena by injecting electrons up to the edge states owing to the strong electron correlations on the flat band as the case of graphene nanoribbon with zigzag edges.

CRediT authorship contribution statement

Susumu Okada: is responsible for the conceptual development of this study. **Nguyen Thanh Cuong**: performed the phonon calculation of the study. **Mina Maruyama**: performed the ab initio molecular dynamics calculation of the study. **Yanlin Gao**: performed the geometric and electronic structure analyses of the study.

Declaration of competing interest

The authors declare that they have no known competing financial interests or personal relationships that could have appeared to influence the work reported in this paper.

Acknowledgement

The authors thank the Japan Science and Technology Agency, Core Research for Evolutionary Science and Technology (JST-CREST; Grant Nos. JPMJCR1715

and JPMJCR20B5) and the Japan Society for the Promotion of Science, Grants-in-Aid for Scientific Research (JSPS KAKENHI; Grant Nos. JP21K14484, JP20K22323, JP20H00316, JP20H02080, JP20K05253, JP20H05664, and JP16H06331), the Joint Research Program on Zero-Emission Energy Research, Institute of Advanced Energy, Kyoto University, and the University of Tsukuba Basic Research Support Program (S). Part of the calculations were performed on an NEC SX-Ace at the Cybermedia Center at Osaka University.

References

[1] G. S. Painter and D. E. Ellis, Electronic Band Structure and Optical Properties of Graphite from a Variational Approach, Phys. Rev. 1 (1970) 4747–4752. https://doi.org/10.1103/PhysRevB.1.4747.

[2] F. Bassani and G. P. Parravicini, Band structure and optical properties of graphite and of the layer compounds GaS and GaSe, Nuovo Cimento B 50 (1967) 95–128. https://doi.org/10.1007/BF02710685.

[3] M. Posternak, A. Baldereschi, A. J. Freeman, E. Wimmer and M. Weinert, Prediction of Electronic Interlayer States in Graphite and Reinterpretation of Alkali Bands in Graphite Intercalation Compounds, Phys. Rev. Lett. 50 (1983) 761–764. https://doi.org/10.1103/PhysRevLett.50.761.

[4] K. S. Novoselov, A. K. Geim, S. V. Morozov, D. Jiang, M. I. Katsnelson, I. V. Grigorieva, S. V. Dubonos, and A. A. Firsov, Two-dimensional gas of massless Dirac fermions in graphene, Nature 438 (2005) 197–200. https://doi.org/10.1038/nature04233.

[5] Y. Zhang, Y. -W. Tan, H. L. Stormer, and P. Kim, Experimental observation of the quantum Hall effect and Berry's phase in graphene, Nature 438 (2005) 201–204. https://doi.org/10.1038/nature04235.

[6] X. Du, I. Skachko, F. Duerr, A. Luican, and E. Y. Andrei, Fractional quantum Hall effect and insulating phase of Dirac electrons in graphene, Nature 462 (2009) 192–195. https://doi.org/10.1038/nature08522.

[7] K. I. Bolotin, F. Ghahari, M. D. Shulman, H. L. Stormer, and P. Kim, Observation of the fractional quantum Hall effect in graphene, Nature 462 (2009) 196–199. https://doi.org/10.1038/nature08582.

[8] N. Shima and H. Aoki, Electronic structure of super-honeycomb systems: A peculiar realization of semimetal/semiconductor classes and ferromagnetism, Phys. Rev. Lett. 71 (1993) 4389–4392. https://doi.org/10.1103/PhysRevLett.71.4389.

[9] Y. Ma, P. O. Lehtinen, A. S. Foster, and R. M. Nieminen, Magnetic properties of vacancies in graphene and single-walled carbon nanotubes, New J. Phys. 6 (2004) 68. https://doi/org/10.1088/1367-2630/6/1/068.

[10] H. Amara, S. Latil, V. Meunier, Ph. Lambin, and J.-C. Charlier, Scanning tunneling microscopy fingerprints of point defects in graphene: A theoretical prediction. Phys. Rev. B 76 (2007) 115423. https://doi.org/10.1103/PhysRevB.76.115423.

[11] M. M. Ugeda, I. Brihuega, F. Hiebel, P, Mallent, J.-Y. Veuillen, J. M. G.-Rodriguez, and F. Yndurain, Electronic and structural characterization

of divacancies in irradiated graphene, Phys. Rev. B 85 (2012)121402(R). https://doi.org/10.1103/PhysRevB.85.121402.

[12] M. Sakurai, Y. Sakai, and S. Saito, Electronic properties of graphene and boron-nitride based nanostructured materials, J. Phys.: Conf. Ser. 302 (2011) 012018. https://doi/org/10.1088/1742-6596/302/1/012018.

[13] M. Maruyama, N. T. Cuong, and S. Okada, Coexistence of Dirac cones and Kagome flat bands in a porous graphene, Carbon 109 (2016) 755–763. https://doi.org/10.1016/j.carbon.2016.08.090.

[14] M. Fujita, K. Wakabayashi, K. Nakada, and K. Kusakabe, Peculiar Localized State at Zigzag Graphite Edge , J. Phys. Soc. Jpn. 65 (1996) 1920–1923. https://doi.org/10.1143/JPSJ.65.1920.

[15] K. Nakada, M. Fujita, G. Dresselhaus, and M. S. Dresselhaus, Edge state in graphene ribbons: Nanometer size effect and edge shape dependence, Phys. Rev. B 54 (1996) 17954–17961. https://doi.org/10.1103/PhysRevB.54.17954.

[16] Y. Miyamoto, K. Nakada, and M. Fujita, First-principles study of edge states of H-terminated graphitic ribbons, Phys. Rev. B 59 (1999) 9858–9861. https://doi.org/10.1103/PhysRevB.59.9858.

[17] S. Okada and A. Oshiyama, Magnetic Ordering in Hexagonally Bonded Sheets with First-Row Elements, Phys. Rev. Lett. 87 (2001) 146803. https://doi.org/10.1103/PhysRevLett.87.146803.

[18] K. Kusakabe, K. Wakabayashi, M. Igami, K. Nakada, and M. Fujita, Magnetism of nanometer-scale graphite with edge or topo-

logical defects, Mol. Cryst. Liq. Cryst. 305 (1997) 445–454. https://doi.org/10.1080/10587259708045079.

[19] J. Fernández-Rossier and J. J. Palacios, Magnetism in graphene nanoislands, Phys. Rev. Lett. 99 (2007) 177204. https://doi.org/10.1103/PhysRevLett.99.177204.

[20] O. V. Yazyev and S. G. Louie, Topological defects in graphene: Dislocations and grain boundaries, Phys. Rev. B 81 (2010) 195420. https://doi.org/10.1103/PhysRevB.81.195420.

[21] S. Okada, T. Kawai, and K. Nakada, Electronic structure of graphene with topological line defect, J. Phys. Soc. Jpn. 80 (2011) 013709. https://doi.org/10.1143/JPSJ.80.013709.

[22] M. Maruyama, S. Okada, A two-dimensional sp^2 carbon network of fused pentagons: All carbon ferromagnetic sheet, Appl. Phys. Express 6 (2013) 095101. https://doi.org/10.7567/APEX.6.095101.

[23] N. Hamada, S. -I. Sawada, and A. Oshiyama, New one-dimensional conductors: graphitic microtubules, Phys. Rev. Lett. 68 (1992) 1579–1581. https://doi.org/10.1103/PhysRevLett.68.1579.

[24] R. Saito, M. Fujita, G. Dresselhaus, and M. S. Dresselhaus, Electronic structure of chiral graphene tubules, Appl. Phys. Lett. 60 (1992) 2204–2206. https://doi.org/10.1063/1.107080.

[25] K. Tanaka, K. Okahara, M. Okada, and T. Yamabe, Electronic properties of bucky-tube model, Chem. Phys. Lett. 191 (1992) 469–472. https://doi.org/10.1016/0009-2614(92)85410-C.

[26] L. Zhi and K. Müllen, A bottom-up approach from molecular nanographenes to unconventional carbon materials, J. Mater. Chem. 18 (2008) 1472–1484. https://doi.org/10.1039/B717585J.

[27] J. Cai, P. Ruffieux, R. Jaafar, M. Bieri, T. Braun, S. Blankenburg, M. Muoth, A. P. Seitsonen, M. Saleh, X. Feng, K. Müllen, Nature 466 (2010) 470. https://doi.org/10.1038/nature09211.

[28] L. Chen, Y. Hernandez, X. Feng, and K. Müllen, From Nanographene and Graphene Nanoribbons to Graphene Sheets: Chemical Synthesis, Angew. Chem. Int. Ed. 51 (2012) 7640–7654. https://doi.org/10.1002/anie.201201084.

[29] A. P. Côté, A. I. Benin, N. W. Ockwig, M. O'Keeffe, A. J. Matzger, and O. M. Yaghi, Porous, crystalline, covalent organic frameworks, Science 310 (2005) 1166–1170. https://doi.org/10.1126/science.1120411.

[30] F. J. Uribe-Romo, J. R. Hunt, H. Furukawa, C. Klöck, M. O'Keeffe, and O. M. Yaghi, A Crystalline Imine-Linked 3-D Porous Covalent Organic Framework, J. Am. Chem. Soc. 131 (2009) 4570–4571. https://doi.org/10.1021/ja8096256.

[31] T. Ben, H. Ren, S. Ma, D. Cao, J. Lan, X. Jing, W. Wang, J. Xu, F. Deng, J. M. Simmons, S. Qiu, and G. Zhu, Targeted synthesis of a porous aromatic framework with high stability and exceptionally high surface area, Angew. Chem. Int. Ed. 48 (2009) 9457–9460. https://doi.org/10.1002/anie.200904637.

[32] W. Lu, D. Yuan, D. Zhao, C. I. Schilling, O. Plietzsch, T. Muller, S. Bräse, J. Guenther, J. Blümel, R. Krishna, Z. Li, and H.-C. Zhou, Porous Polymer Networks: Synthesis, Porosity, and Applications in Gas Storage/Separation, Chem. Mater. 22 (2010) 5964–5972. https://doi.org/10.1021/cm1021068.

[33] R. Mitschka, J. Oehldrich, K. Takahashi, J. M. Cook, U.Weiss, and J. V. Silverton, General approach for the synthesis of polyquinanes. Facile generation of molecular complexity via reaction of 1,2-dicarbonyl compounds with dimethyl 3-, Tetrahedron 37 (1981) 4521–4542. https://doi.org/10.1016/0040-4020(81)80020-8.

[34] M. N. Deshpande, M. Jawdosiuk, G. Kubiak, M. Venkatachalam, U. Weiss, and J. M. Cook, General approach for the synthesis of polyquinenes. 2. Synthesis of tetracyclo[5.5.1.04,13.010,13]tridecane-2,5,8,11-tetraene, J. Am. Chem. Soc. 107 (1985) 4786–4788. https://doi.org/10.1021/ja00302a035.

[35] M. Venkatachalam, M. N. Deshpande, M. Jawdosiuk, G. Kubiak, S. Wehrli, J. M. Cook, and U. Weiss, General approach for the synthesis of polyquinenes, Tetrahedron 42 (1986) 1597–1605. https://doi.org/10.1016/S0040-4020(01)87576-1.

[36] B. Bredenkötter, B. Neumann, H.-G. Stammler, and Dietmar Kuck, Phenanthro-Annelated [5.5.6.6]- and (Broken) [6.5.6]Fenestranes, Eur. J. Org. Chem. (2014) 53–65. https://doi.org/10.1002/ejoc.201301382.

[37] W.-S. Wong, Ch.-F. Ng, D. Kuck, and H.-F. Chow, From Fenestrindane towards Saddle-Shaped Nanographenes Bearing a Tetracoor-

dinate Carbon Atom, Angew. Chem. Int. Ed. 56 (2017) 12356–12360. https://doi.org/10.1002/anie.201707505.

[38] W.-S. Wong, H.-W. Tse, E. Cheung, D. Kuck, and H.-F. Chow, Enantiopure Aromatic Saddles Bearing the Fenestrindane Core, J. Org. Chem. 84 (2019) 869–878. https://doi.org/10.1021/acs.joc.8b02719.

[39] P. Hohenberg and W. Kohn, Inhomogeneous Electron Gas, Phys. Rev. 136 (1964) B864–B871. https://doi.org/10.1103/PhysRev.136.B864.

[40] W. Kohn and L. J. Sham, Self-Consistent Equations Including Exchange and Correlation Effects, Phys. Rev. 140 (1965) A1133–A1138. https://doi.org/10.1103/PhysRev.140.A1133.

[41] Y. Morikawa, K. Iwata, and K. Terakura, Theoretical study of hydrogenation process of formate on clean and Zn deposited Cu(111) surfaces, Appl. Surf. Sci. 169-170 (2001) 11–15. https://doi.org/10.1016/S0169-4332(00)00631-0.

[42] A simulation tool for atom technology (STATE): https://state-doc.readthedocs.io/en/latest/index.html

[43] P. Giannozzi et al., QUANTUM ESPRESSO: a modular and open-source software project for quantum simulations of materials, J. Phys.: Condens. Mater. 21(2009) 395502. https://doi.org/10.1088/0953-8984/21/39/395502.

[44] J. P. Perdew, K. Burke, and M. Ernzerhof, Generalized Gradient Approximation Made Simple, Phys. Rev. Lett. 77 (1996) 3865–3868. https://doi.org/10.1103/PhysRevLett.77.3865.

[45] D. Vanderbilt, Soft self-consistent pseudopotentials in a generalized eigenvalue formalism, Phys. Rev. B 41 (1990) 7892–7895. https://doi.org/10.1103/PhysRevB.41.7892.

[46] M. F. Semmelhack, J. S. Foos, and S. Katz, Spiro[4,4]nonatetraene and spiro[4,4]nona-1,3,7-triene, J. Am. Chem. Soc. 94 (1972) 8637–8638. https://doi.org/10.1021/ja00779a088.

[47] M. F. Semmelhack, J. S. Foos, and S. Katz, Spiro[4.4]nonatetraene and spiro[4.4]nona-1,3,7-triene. Synthesis and properties. Effects of spiroconjugation, J. Am. Chem. Soc. 95 (1973) 7325–7336. https://doi.org/10.1021/ja00803a021.

[48] O. Ohara, C. Aso, and T. Kunitake, Studies on Polymers from Cyclic Dienes. XIII. Cationic Polymerization of Spiro[4,4]nona-1,3-diene, Polymer J. 5 (1973) 49–54. https://doi.org/10.1295/polymj.5.49.

[49] S. Baroni, S. de Gironcoli, A. D. Corso, and P. Giannozzi, Phonons and related crystal properties from density-functional perturbation theory, Rev. Mod. Phys. 73 (2001) 515–562. https://doi.org/10.1103/RevModPhys.73.515

[50] B. Ram and H. Mizuseki, Tetrahexcarbon: A two-dimensional allotrope of carbon, Carbon 137 (2018) 266–273. https://doi.org/10.1016/j.carbon.2018.05.034.

[51] B. Ram and H. Mizuseki, C_{568}: A new two-dimensional sp^2-sp^3 hybridized allotrope of carbon, Carbon 158 (2020) 827–835. https://doi.org/10.1016/j.carbon.2019.11.062.

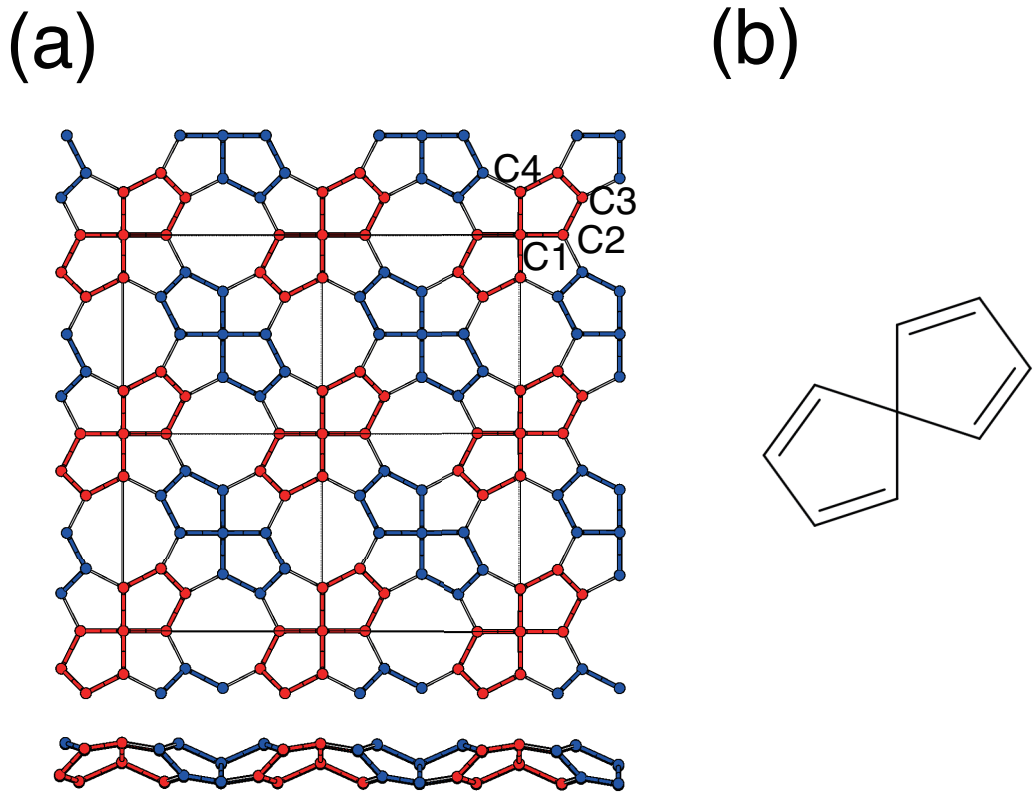

Figure 1: (a) Top and side views of an optimized atomic structure of polymerized spiro[4,4]nonatetraene. The red and blue pentagons corresponded to the spiro[4,4]nonatetraene unit with different orientations, the solid squares indicate the unit cell boundaries, and the indexes indicate independent atomic sites under the symmetry of *Pmmn*. (b) A molecular structure of spiro[4,4]nonatetraene.

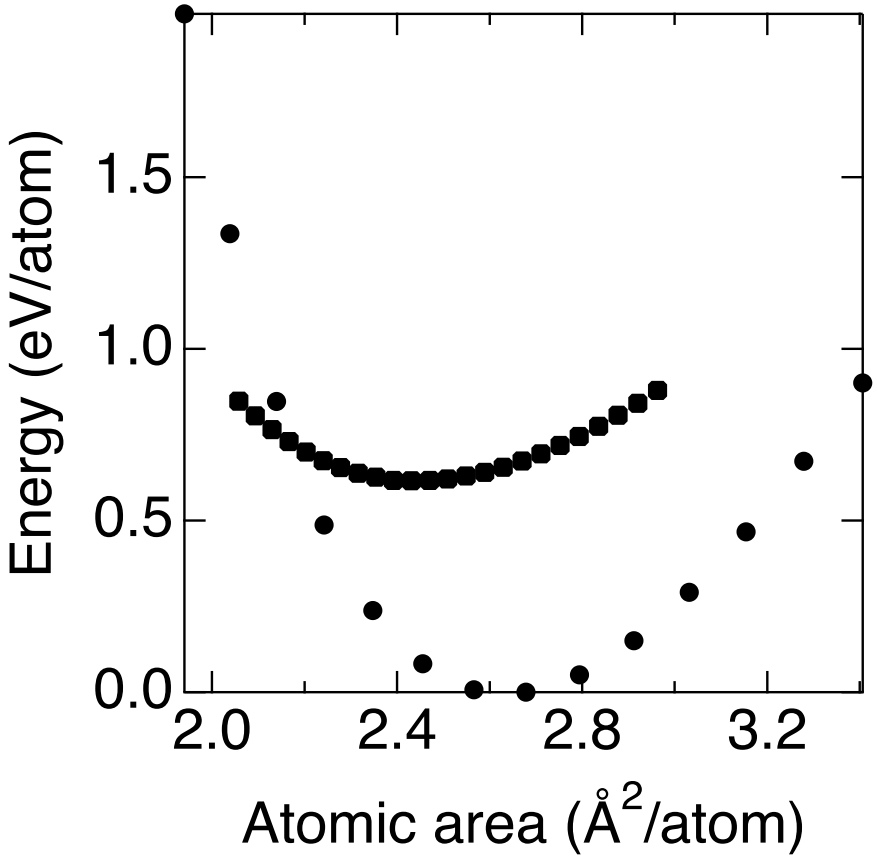

Figure 2: Relative energy of polymerized spiro[4,4]nonatetraene per atom as a function of atomic area. The total energy of graphene per atom as a function of atomic area is also plotted. Squares and circles indicate the energies of polymerized spiro[4,4]nonatetraene and graphene, respectively. The energy is measured from that of graphene with an equilibrium lattice constant.

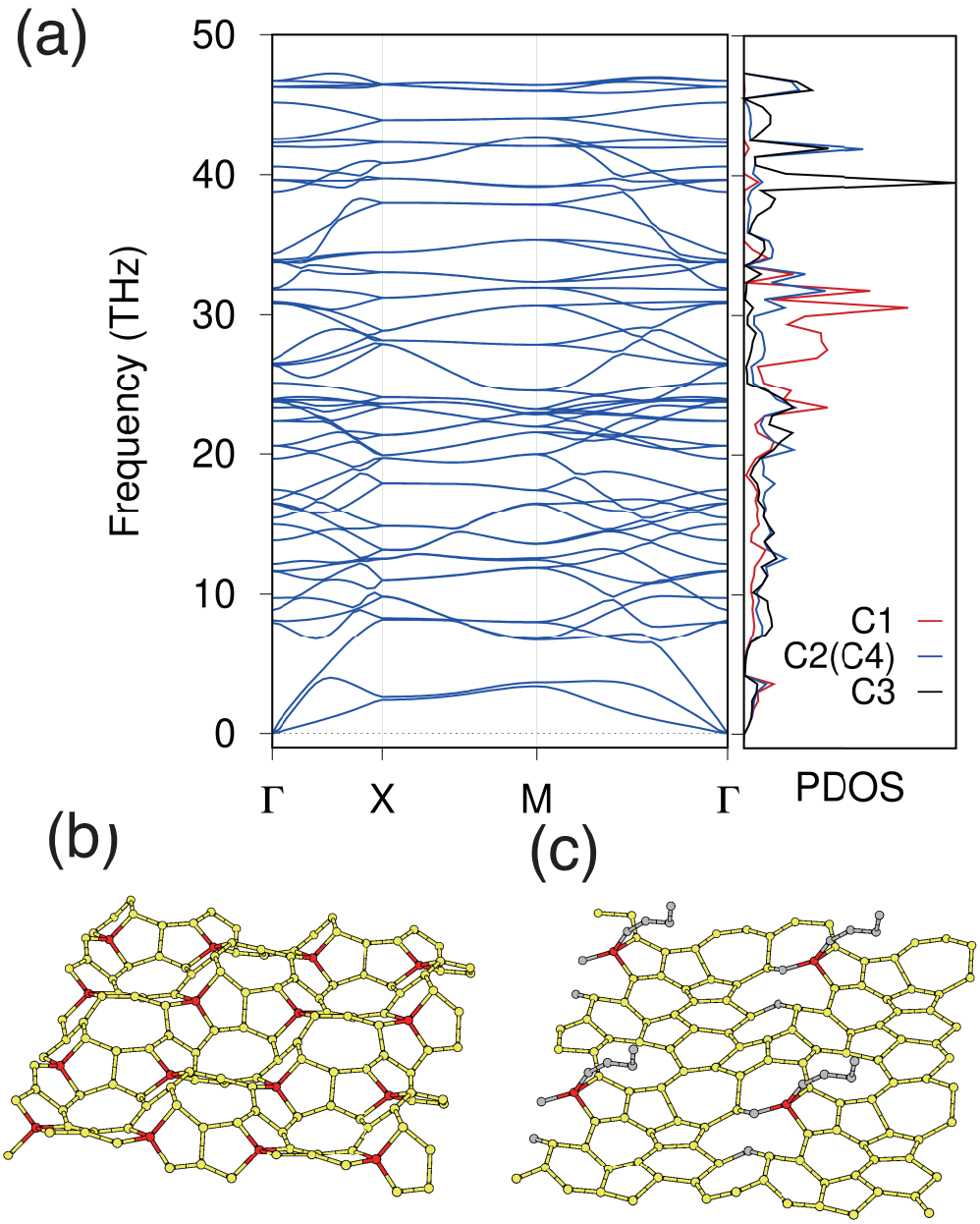

Figure 3: (a) Phonon dispersion and phonon density of states of polymerized spiro[4,4]nonatetraene. Snapshots of the polymerized spiro[4,4]nonatetraene (b) at T = 2000 K and (c) at T = 4000 K after 10 ps of MD simulation time. Yellow, red, and gray balls indicate C atoms with three, four, and one or two coordinations, respectively.

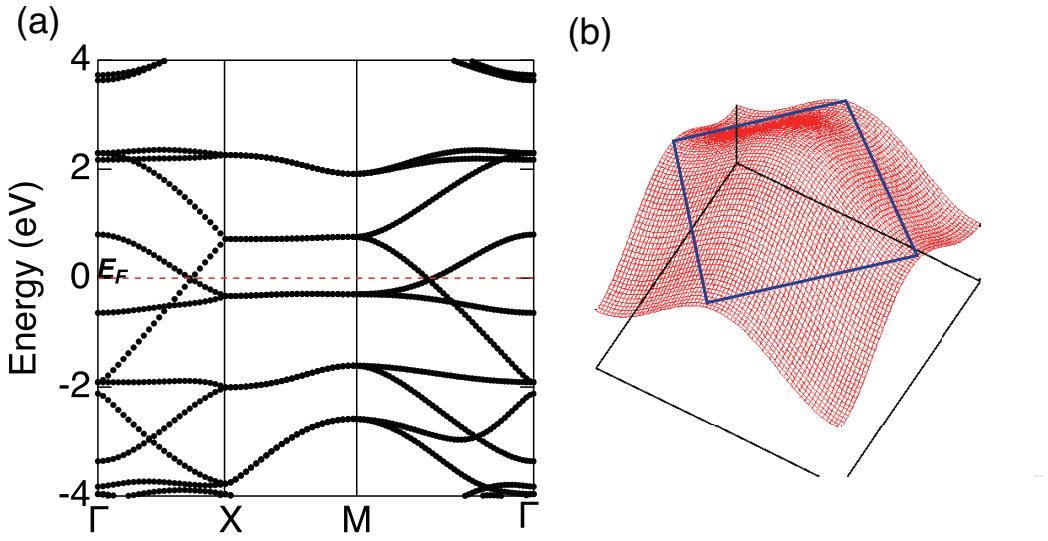

Figure 4: (a) The electronic band structure of polymerized spiro[4,4]nonatetraene along the high symmetry points and lines. Energies are measured from the Fermi level, which is denoted by the horizontal dotted line. (b) Two-dimensional cosine band of a square lattice. The black and blue lines denote the Brillouin zone with 1×1 cell and $\sqrt{2} \times \sqrt{2}$ cell, respectively.

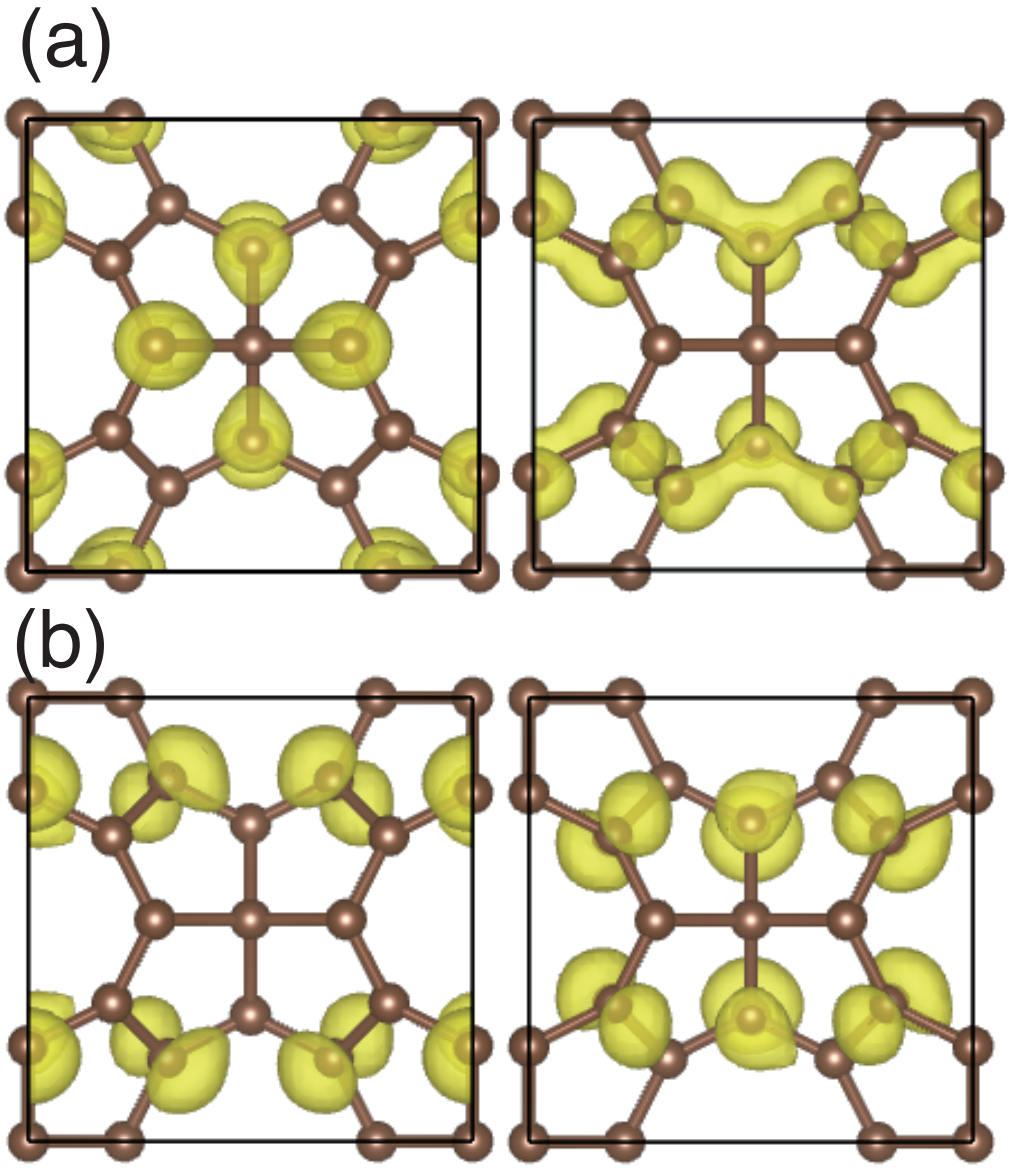

Figure 5: Isosurfaces of squared wave functions of (a) the pseudo-Dirac point at the middle of the Γ-X line and (b) the Dirac point at the X point in Fig. 4.

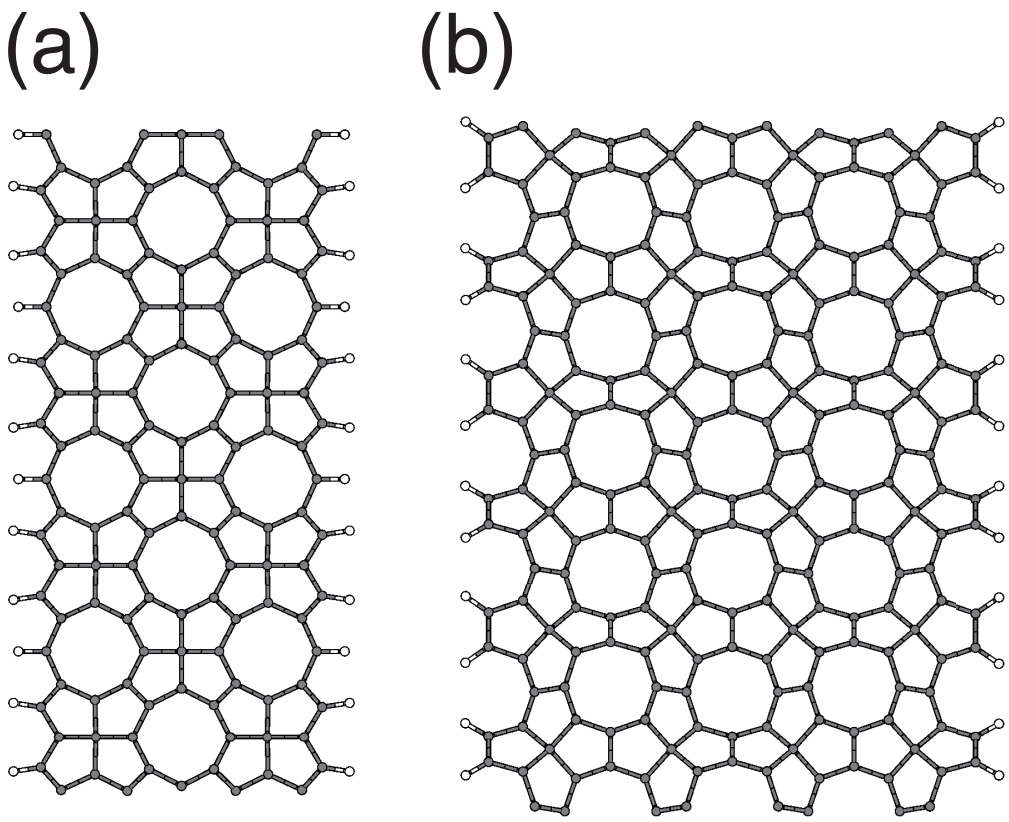

Figure 6: Optimized structures of polymerized spiro[4,4]nonatetraene nanoribbons with (a) zigzag and (b) armchair edges. The gray and white balls indicate C and H atoms, respectively. The ribbons are extended along the vertical direction.

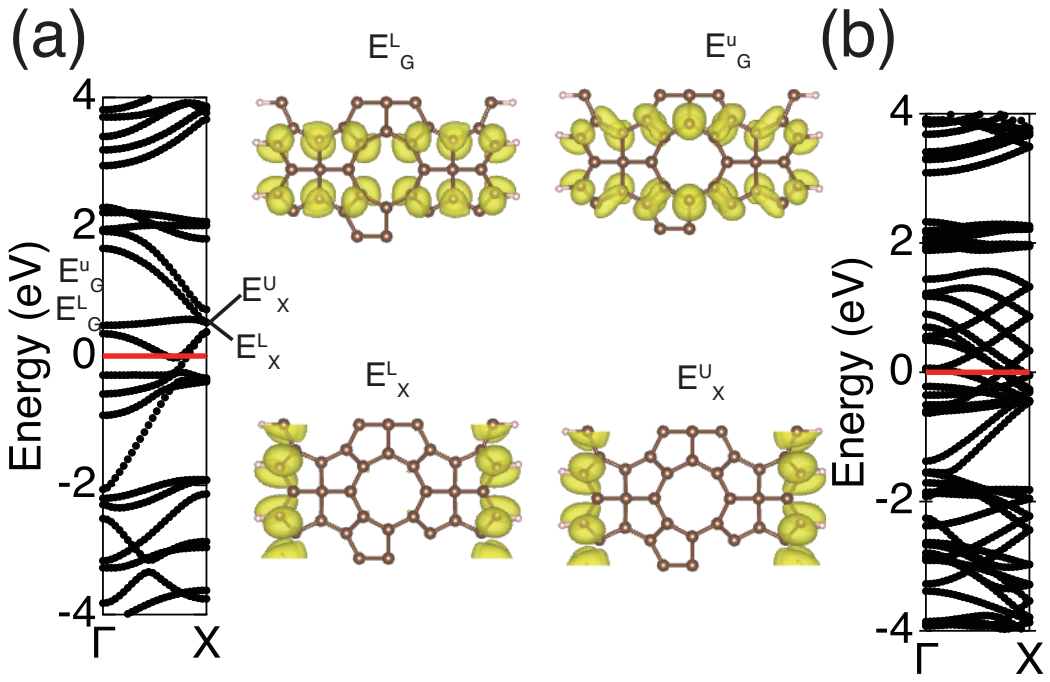

Figure 7: Electronic structures of polymerized spiro[4,4]nonatetraene nanoribbons with (a) zigzag and (b) armchair edges. The red horizontal lines indicate the Fermi level. The squared wave functions of the states associated with the edge states are also shown in the right of Fig. 7(a). E_G^L, E_G^U, E_X^L, and E_X^U indicate the wave functions of the lower edge state at the Γ point, the upper edge state at the Γ point, the lower edge state at the X point, and the upper edge state at the X point, respectively. These indexes are labeled in Fig. 7(a).